

On the relative role of upslope and downslope topography for describing water flow path and storage dynamics: a theoretical analysis

C. Lanni,^{1,2*} J. J. McDonnell² and R. Rigon¹

¹ Department of Civil and Environmental Engineering, University of Trento, Trento, Italy

² Department of Forest Engineering, Resources & Management, Oregon State University, Corvallis, OR, USA

Abstract:

Many current conceptual rainfall-runoff and shallow landslide stability models are based on the topographic index concept derived from the steady-state assumption for subsurface water flow dynamics and the hypothesis that the surface gradient is a good approximation for the gradient of the total hydraulic head. However, increasing field evidence from sites around the world has shown poor correlations between the topographic index and the patterns of soil water storage. Here we present a new, smoothed, dynamic topographic index and test the ability of this index to reproduce spatial patterns of wetness areas and storage as provided by a distributed, physically based, Boussinesq equation (BEq) solver. Our results show that the new smoothed dynamic topographic index outperforms previous, locally computed indices in the estimation of storage dynamics, resulting in less fragmented and disconnected spatial patterns of storage. Our new dynamic index is able to capture both the upslope and downslope controls on water flow and approximates storage dynamics across scales. The new index is compatible with high-resolution topographic data. We encourage the use of our smoothed dynamic topographic index to describe the lateral subsurface flow component in landslide generation models and conceptual rainfall-runoff models, especially when high-resolution digital elevation models are available. Copyright © 2011 John Wiley & Sons, Ltd.

KEY WORDS topographic wetness index; storage dynamics; hydrological connectivity; flow paths; distributed hydrological model; rainfall-runoff models

Received 14 February 2011; Accepted 8 August 2011

INTRODUCTION

The use of digital elevation data to calculate water flow paths has been a central focus of hydrological modelling ever since the development of the area-slope index in geomorphology (Carson and Kirkby, 1972) and the topographic wetness index (TWI) in hydrology (Kirkby, 1975). These indices have been largely used to infer the water storage in the entire catchment area (e.g. Lamb *et al.*, 1998), the extension of saturated areas (e.g. Grabs *et al.*, 2009) and as general indicators of the influence of topography on soil–water storage dynamics (e.g. McGuire *et al.*, 2005; Tetzlaff *et al.*, 2009a,b).

The traditional topographic index (Kirkby, 1975) is normally calculated, by digital terrain analysis, as the natural logarithm of the ratio between the drained area per unit contour length, a , and the slope of the ground surface at the location, $\tan\beta$: $\text{TWI} = \log(a/\tan\beta)$. Beven and Kirkby (1979) developed the topographic index into a terrain analysis-based hydrologic model (TOPMODEL), which is able to produce a simple relation of soil–water storage (deficit) in a catchment. This model expresses the local storage deficit below saturation by assuming that the major factor affecting the water flow paths is the catchment topography:

$$Z = -\frac{1}{f}(\text{TWI} + \log(R) - \log(T)) \quad (1)$$

where R [LT^{-1}] is the net vertical recharge (i.e. the rainfall intensity minus the sum of evapotranspiration and bedrock leakage) usually assumed spatially uniform, T [L^2T^{-1}] is the maximum soil transmissivity, obtained when the groundwater level is at the ground surface, f [L] is a parameter controlling the rate of decline of transmissivity with increasing storage deficit, and Z [L] is the local storage deficit below saturation expressed as water table depth from the ground surface.

Table I summarises the algorithms that have been developed to compute the TWI since the early 1980s (Table I). Early work augmented the TWI from a single flow path direction to a multiflow directional algorithm to capture the smearing of flow downslope produced by multiple partial flow path weighting (e.g. Quinn *et al.*, 1991; Tarboton, 1997; Seibert and McGlynn, 2007). The main premise of each of the TWI variants is that elevation potential dominates total hydraulic potential, and hence topography is a good proxy for representing subsurface flow paths and soil–water storage dynamics. This is generally the case in mountain regions with moderate to steep topography (Tetzlaff *et al.*, 2009a), where a shallow (highly conductive) soil layer lies on an impervious bedrock substrate (Western *et al.*, 2004). However, field-

*Correspondence to: Lanni, Cristiano, Civil and Environmental Engineering, University of Trento, Trento 38123, Italy.
E-mail: cristiano.lanni@gmail.com

Table I. A list of the major efforts of the last 30 years to produce more realistic terrain indices from digital elevation models

No.	Authors	Year	Terrain index investigated	Improvement efforts focused upon	Method
1	Beven and Kirkby	1979	TWI		
2	O'Callaghan and Mark	1984	a	a	Single flow direction (D8)
3	Quinn et al.	1991	a	a	Multiple flow directions
4	Barling et al.	1994	a	a	Time-variable upslope area, $a(t)$
5	Tarboton	1997	a	a	Infinite possible single-direction flow pathways ($D\infty$)
6	Beven and Freer	2001	TWI	a	Time-variable upslope area, $a(t)$
7	Borga et al.	2002	TWI	a	Time-variable upslope area, $a(t)$
8	Orlandini et al.	2003	a	a	Path-based method considering cumulative deviation from the steepest directions (D8-LTD)
9	Hjerdt et al.	2004	$\tan\beta$	$\tan\beta$	Downslope index, DWI
10	Seibert and McGlynn	2007	a	a	Combination of multiple flow and $D\infty$ (MD ∞)

based testing of the TWI has shown weak relations with soil moisture patterns (Burt and Butcher, 1986; Seibert et al., 1997; Lamb et al., 1998; Western et al., 1999) and often poor correlations with shallow groundwater levels (Iorgulescu and Jordan, 1994; Jordan, 1994).

Some studies have also questioned the fundamental assumptions of the topographic index theory (Burt and Butcher, 1985; Crave and Gascuel-Odoux, 1997; Seibert et al., 1997; Pellenq et al., 2003; Hjerdt et al., 2004). Two of these assumptions are of widespread use: (i) the hypothesis of steady-state subsurface flow, where time-dependent storage terms are neglected, and (ii) the validity of the kinematic-wave equation (KWeq) used to describe the subsurface water flow. The latter is an approximation of the BEq in which, however, the diffusive term depending on hydrostatic pressure gradients is neglected and the hydraulic gradient is approximated with the slope of the topographic surface. The KWeq can therefore only propagate the effects of disturbances in a downslope direction, and it cannot predict any backwater effect induced by complex dynamical organisation of flow paths.

Barling et al. (1994) were the first to deal with the problem of the steady-state assumption of flow, arguing that rainfall events are seldom sufficient to bring a hillslope to the steady-state condition. This motivated the development of their quasi-dynamic TWI with a time-variable upslope contributing area. They showed that the quasi-dynamic index was in closer agreement with the measured pattern of soil moisture storage than the traditional steady-state TWI.

Notwithstanding these advancements, in Barling et al. (1994) and successive studies, most of the developments in TWI to date have focused on new ways to compute specific upslope contributing area (O'Callaghan and Mark, 1984; Quinn et al., 1991; Tarboton, 1997; Orlandini et al., 2003; Seibert and McGlynn, 2007) or time-variable upslope contributing area (Barling et al., 1994; Beven and Freer, 2001; Borga et al., 2002). Local slope, $\tan\beta$, continued to

be assumed a good surrogate to describe the local drainage propensity.

One exception has been the development of the downslope wetness index, or drainage efficiency index, $DWI = d / L_d$, where L_d represents how far a particle of water has to travel along its flow path to lose a given head potential, d . Hjerdt et al. (2004) showed how this DWI outperformed the standard topographic index for mapping mire distribution in Sweden and approximating soil nitrate patterns and soil depths in headwater catchments in the USA. Nevertheless, the subsequent use of the downslope index has shown equivocal results (e.g. Güntner et al. 2004; Grabs et al. 2009).

Clearly, the metrics of local slope need to be improved to better approximate both upslope and downslope controls on water flow, storage deficit and resulting connectivity (i.e. the condition by which disparate wetter zones on the watershed are linked via subsurface water flow; e.g. Stieglitz et al., 2003) in the landscape. At present, no theoretical approach exists for characterising the relative role of upslope and downslope topography for describing water flow path, connectivity and storage across scales. Here we develop a new terrain-based index to include the relative role of upslope and downslope topography and (at least partially) overcome the limitations found in traditional topographic indices. We present a theoretical proof-of-concept analysis where the predictions of the new index and several other topographic indices are compared against patterns of water storage deficit (or water table depth) provided by a physically based model that describes the subsurface lateral flow dynamics obtained by solving the BEq. We then explore how gradients of pressure head, induced by the downslope topography constraints, affect water storage dynamics and flow pathways organisation. Our goal is to preserve the simple formulation and low computational demand that characterises the use of popular, terrain-based indices, while at the same time combine elements of the upslope and downslope topography that smooth the

influence of terrain on water flow. We expand upon Barling (1994) dynamic index concept to deal with past issues of local slope, overestimation of local hydraulic gradient (e.g. Crave and Gascuel-Odoux, 1997; Haitjema and Mitchell-Bruker, 2005) and (nonphysical) fragmentation of the patterns (e.g. Lane *et al.*, 2004; Sørensen and Seibert, 2007), especially when high-resolution DEM are analysed.

MATERIALS AND METHODS

Study site

Our study site is the 3.2-km² Salei alpine catchment in northern Italy. A 2-m resolution DEM (with a total of 791636 cells) of the Salei basin was developed from LiDAR data.

The catchment elevation ranges from 1700 to 2400 m above sea level. The average slope is 30°, with a substantial number of slopes that locally exceed 35°. A shallow sandy-silt, nonlayered soil (varying in depth from a few centimetres to 1–1.5 m), with medium–high saturated hydraulic conductivity ($K_{\text{sat}} = 10^{-4}$ m/s) and soil porosity $\phi = 0.3 \text{ m}^3 \text{ m}^{-3}$ (based on field observation by E. Farabegoli, personal communication), covers the underlying bedrock. This bedrock consists of poorly fractured volcaniclastic conglomerates throughout the entire basin area. Annual precipitation is approximately 1000 mm (source: Meteo Trentino, Provincia Autonoma di Trento).

The catchment is characterised by two sub-basins, where steep hillslopes converge in two main central hollows. Topography represents a first-order control for soil moisture patterns and subsurface flow paths as we have geological field evidence (by E. Farabegoli, personal communication) that transient water tables develop at the soil–bedrock interface, generating relevant lateral flow during rainfall events. Terrain-based indices are therefore suitable to describe flow paths and storage dynamics at the Salei catchment, as also reported and detailed in other studies (Borga *et al.*, 2008, and 2002; Tarolli *et al.*, 2008; Orlandini and Moretti, 2009).

The watershed has been also used for shallow landslide studies (unpublished) by the authors of this article. A comparison between patterns of slope instability predicted by the SHALSTAB model (Montgomery and Dietrich, 1994), GEOTop (e.g. Rigon *et al.*, 2006) and inventoried landslide areas in the basin have highlighted the need to describe the transient nature of the subsurface flow mechanisms. The steady-state hypothesis used in SHALSTAB (similar to the TOPMODEL one) to simulate the hydrological control (i.e. the water table spatial patterns) on the triggering of shallow landslides leads to an overestimate of slope instability in the basin and does not provide any information on the critical rainfall duration (i.e. the minimum rainfall duration needed to cause slope instability—e.g. Borga *et al.*, 2002). This motivated us to use the Salei basin for our theoretical analysis and index development.

Figure 1 shows the basic hydrological attributes used to define the new terrain-based index. Maps of the drainage

directions (Figure 1a) were evaluated according to the path-based single flow direction method of Orlandini *et al.* (2003). This method was preferred over other methods (e.g. Quinn *et al.*, 1991; Tarboton, 1997; Seibert and McGlynn, 2007) because it was shown to provide a better representation of flow paths across the surface of the Salei basin (Orlandini and Moretti, 2009; Gallant and Hutchinson, 2011). The drainage directions were coded by using a number between 1 and 8. A value of 1 indicates that the water particle moves eastward, a value of 2 indicates that the water particle moves northeasterly, and so on, going counterclockwise.

The two-dimensional BEq model

We used the numerical model BEq of Cordano and Rigon (submitted) to simulate flow paths, water table levels (i.e. storage deficit) and connectivity across the Salei catchment in response to three different rainfall events. The simulated rainfall events were characterised by the rainfall intensity (2, 4 and 8 mm h⁻¹, respectively) and the rainfall duration (16, 16 and 8 h, respectively). These events correspond to events with a return period of 1 to 10 years; therefore, they can be considered ‘typical’ of the site.

The results were then used to compare the performance of several terrain-based indices. The BEq model solves the following two-dimensional form of the BEq (Bear, 1972):

$$\Phi(x, y) \frac{\partial h}{\partial t} = \nabla \left[K_{\text{sat}}(x, y, z) \psi(h, x, y) \vec{\nabla} h \right] + Q(x, y) \quad (2)$$

where h [L] is the hydraulic head (i.e. the water table elevation) and ψ [L] is the pressure head, which is a function of h and space: $\psi = \max(0, h - z_b(x, y))$, where $z_b(x, y)$ [L] is the bedrock elevation, t [T] is the time, $\nabla \cdot$ is the divergence operator, $\vec{\nabla}$ is the space gradient operator, $Q(x, y)$ [LT⁻¹] is a source term (e.g. the net rainfall intensity), which also accounts for boundary conditions (for instance the bedrock leakages), K_{sat} [LT⁻¹] is the saturated hydraulic conductivity and $\Phi(x, y)$ [–] is the soil porosity. The BEq model integrates each grid element, taking into account the local variability of both topography and soil properties by a subgrid parameterisation (for further information on the numerical scheme, download BEq on <http://www.geotop.org/cgi-bin/moin.cgi/Boussinesq>, or refer to Brugnano and Casulli, 2009).

Unlike the KWeq, BEq does not neglect the diffusive term (i.e. the gradient of the pressure head $\rightarrow \psi$) in the governing equations. Such process representation is therefore able to account for the enhancement or impedance of local drainage by downslope topography that has been generally neglected in previous studies (e.g. Barling *et al.*, 1994; Grabs *et al.*, 2009), where topographic indices were compared against patterns of water storage from KWeq-based hydrological.

The setting of the terrain-based indices

The ability of the new wetness index TWI_d^* , defined below to approximate the BEq-derived water table patterns,

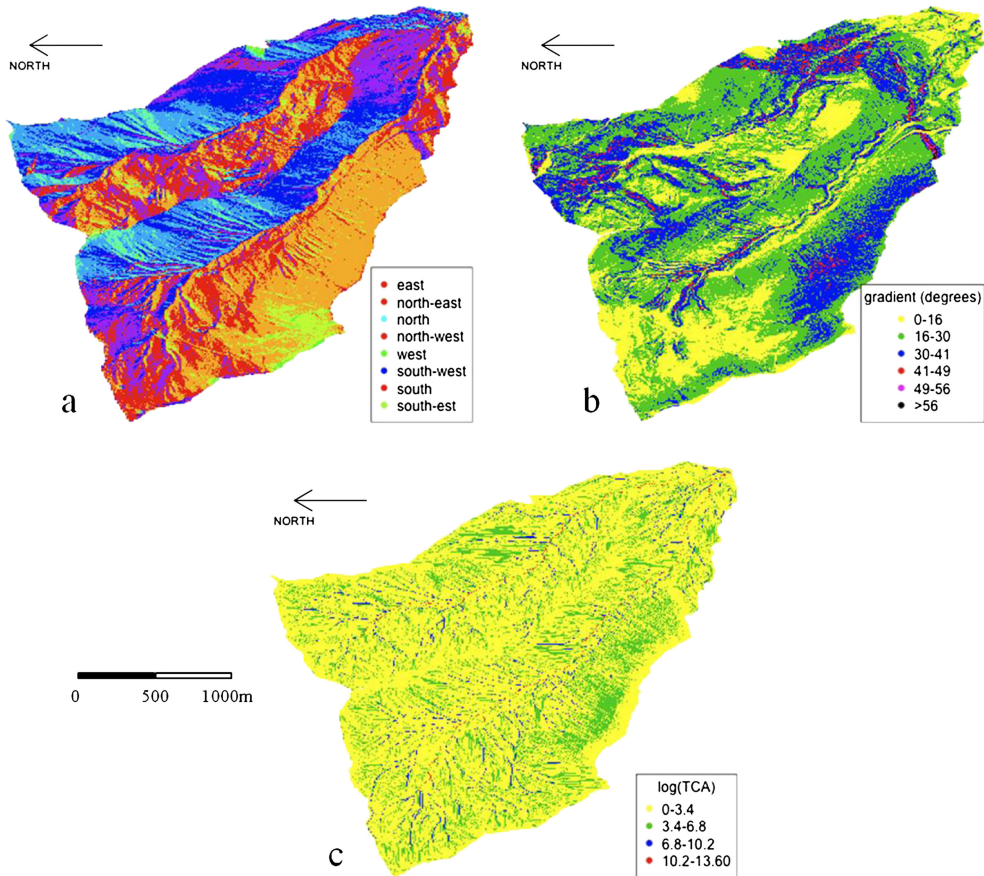


Figure 1. Maps of (a) topographic drainage directions, (b) local slope $\tan\beta$ and (c) upslope contributing area A of the Salei catchment. The upslope contributing area is mapped as the natural logarithm of the area in square metre

was compared against the performance of five other topographic indices (Table II).

Index 1 in Table II, $TWI = \log(a/\tan\beta)$, is the traditional topographic index (Beven and Kirkby, 1979) founded on the assumption of steady-state and local parallelism between ground and water table surfaces. It is defined as the natural logarithm of the ratio between the specific upslope contributing area a (here computed with the path-based single flow routing algorithm D8-LTD of Orlandini *et al.*, 2003) and the local slope, $\tan\beta$.

Index 2, TWI_d , is a dynamic topographic index, which relaxes the hypothesis of steady state by considering a time linear-variable upslope contributing area $A(t)$. The scenario shown in Figure 2 highlights the importance of considering the time-variable upslope contributing area to describe rainfall-runoff processes. In this example, two points, f and b , are located along the same drainage path. Point b (located downslope) presents a value of upslope contributing area larger than point f ($A_b > A_f$). Irrespective of the greater upslope contributing area, point b may actually be 'recharged' by a smaller area than point f during a rainfall event of short duration because of the upslope geomorphology. Hence, for a given duration T_c during a rainfall event, the effective (time-variable) upslope contributing area of point f , $A_f(t)$, may be larger than the effective upslope contributing area of point b , $A_b(t)$.

Table II. The six terrain-based indices defined in this study and their major features

Index	Label	Formulation	Notes
1	TWI	$\log\left(\frac{A/b}{\tan\beta}\right)$	Steady-state upslope contributing area by D8-LTD; hydraulic gradient = local surface slope
2	TWI_d	$\log\left(\frac{A(t)/b}{\tan\beta}\right)$	Time-variable upslope contributing area by D8-LTD; hydraulic gradient = local surface slope
3	TWI_d^{DWI}	$\log\left(\frac{A(t)/b}{DWI}\right)$	Time-variable upslope contributing area by D8-LTD; hydraulic gradient = downslope index
4	TWI_d^*	$\frac{1}{9} \left(TWI_d + \sum_{n=1}^8 TWI_{d_n} \right)$	As Index 2 with 3×3 low-pass filter
5	TWI^*	$\frac{1}{9} \left(TWI + \sum_{n=1}^8 TWI_n \right)$	As Index 1 with 3×3 low-pass filter
6	TWI^{mf}	$\log\left(\frac{A^{mf}/b}{\tan\beta}\right)$	Time-variable upslope contributing area by MF; hydraulic gradient = local surface slope

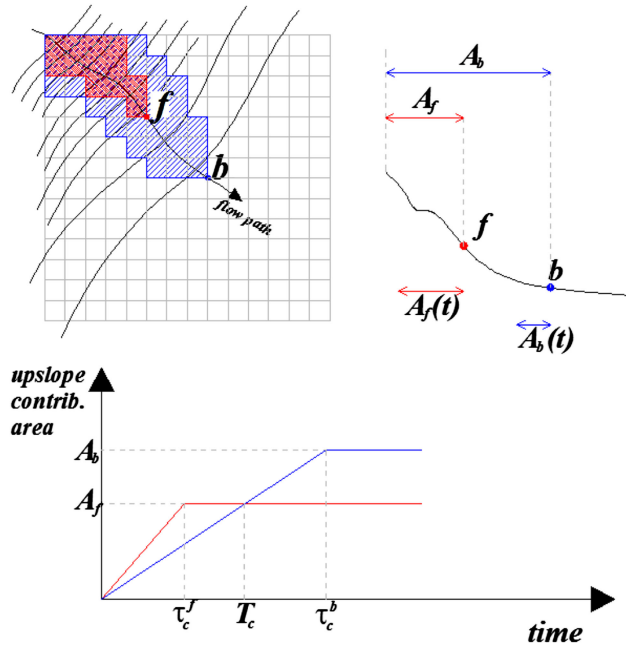


Figure 2. An example of time-variable upslope contributing area. Regardless of their steady-state upslope contributing area A , during a rainfall event the effective (time-variable) upslope contributing area, $A_f(t)$, of a point f located upslope may be larger than the effective (time-variable) upslope contributing area, $A_b(t)$, of a point b located downslope along the same flow path

We described the time-variable upslope contributing area mathematically by using the following linear model:

$$\begin{aligned} A_i(t) &= \frac{t}{\tau_{c_i}} A_i \quad \text{for } t \leq \tau_{c_i} \\ A_i(t) &= A_i \quad \text{for } \tau_{c_i} \leq t \leq D \\ A_i(t) &= \max \left[0, A_i \left(1 + \frac{D-t}{\tau_{c_i}} \right) \right] \quad \text{for } t \geq D (\text{if } \tau_{c_i} \leq D) \\ A_i(t) &= \max \left[0, A_i \left(\frac{2D-t}{\tau_{c_i}} \right) \right] \quad \text{for } t \geq D (\text{if } \tau_{c_i} \geq D) \end{aligned} \quad (3)$$

where $A_i(t)$ and A_i are, respectively, the time-variable upslope contributing area and the (steady-state) upslope contributing area in a given location i , t [T] is the time, D [T] is the rainfall duration and τ_{c_i} [T] is the time of concentration of point i (i.e. the time required for a drop of water to travel from the most hydrologically remote location in the subcatchment to point i). Using Equation 3, the dynamic topographic index TWI_{d_i} (Index 2 in Table II) in a generic point i can be written as

$$\text{TWI}_{d_i} = \log \left(\frac{A_i(t)/b_i}{\tan \beta_i} \right) \quad (4)$$

Equation 3 requires knowledge of τ_{c_i} for each point in a catchment.

We evaluated τ_{c_i} as the maximum ratio between the flow-path length and the celerity of water given by Darcy's law:

$$\tau_{c_i} = \left[\frac{l_{H_j}}{\cos(\alpha_{l_{H_j}})} \cdot \frac{\Phi}{K_{\text{sat}}} \right]_{\max} \quad (5)$$

where $\alpha_{l_{H_j}}$ is the average inclination angle of a given flow path, j , of horizontal length l_{H_j} , which converges in the

generic watershed point i . If both soil porosity, Φ , and saturated hydraulic conductivity, K_{sat} , are assumed constant in space, then Equation 5 becomes

$$\tau_{c_i} = \left[\frac{l_{H_j}}{\cos(\alpha_{l_{H_j}})} \right]_{\max} \cdot \frac{\Phi}{K_{\text{sat}}} = L_{H_i} \cdot \frac{\Phi}{K_{\text{sat}}} \quad (6)$$

where L_{H_i} is a morphological ratio defining the longest flow path of a water particle that converges at the generic watershed point i .

By using the same Equation 3, we defined the $\text{TWI}_d^{\text{DWI}}$ (Index 3 in Table II) by replacing the local slope, $\tan \beta$, with the downslope index, DWI, in Equation 4:

$$\text{TWI}_d^{\text{DWI}} = \log \left(\frac{A_i(t)/b_i}{\text{DWI}_i} \right) \quad (7)$$

$\text{TWI}_d^{\text{DWI}}$ relaxes the hypothesis of parallelism between ground and water table surfaces. Three values of d were selected to define DWI: $d=2$ m, $d=5$ m and $d=10$ m. The DWI for a generic point i was evaluated as the slope of the line that connects the point i with the first point located d -metres below the elevation of point i . This was carried out by assuming that the drop of water travels along the topographic drainage direction (Figure 3).

The new smoothed dynamic index $\text{TWI}_{d_i}^*$ (Index 4 in Table II), was obtained by applying a 3×3 low-pass filter to the map of the dynamic wetness index TWI_d (i.e. by replacing the dynamic wetness index at cell i , TWI_{d_i} , with the average value from the surrounding n-cells):

$$\text{TWI}_{d_i}^* = \frac{1}{9} \left(\text{TWI}_{d_i} + \sum_{n=1}^8 \text{TWI}_{d_n} \right) \quad (8)$$

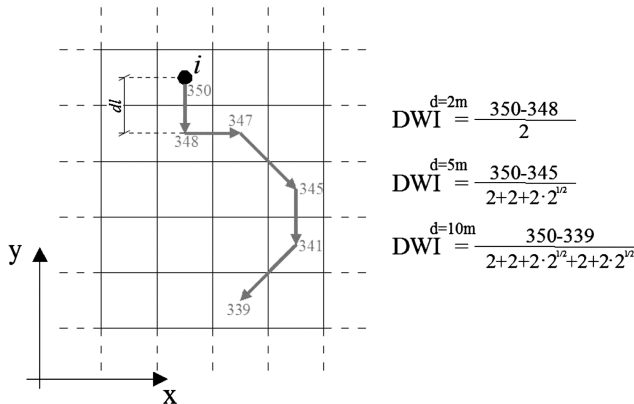


Figure 3. Value of DWI for a point i and three values of d (2, 5 and 10 m). The numbers inside cells are elevations (expressed in metres), arrows represent topographic drainage directions and dl (2 m) is the DEM resolution

The 3×3 low-pass filter increases the spatial autocorrelation of the terrain index by smoothing out local variations in the spatial distribution of the dynamic wetness index TWI_d .

TWI^* (Index 5 in Table II) is a modified version of the traditional topographic index, where the 3×3 low-pass filter is applied on the TWI's map to consider the effect of nonlocal topography:

$$\text{TWI}^* = \frac{1}{9} \left(\text{TWI}_i + \sum_{n=1}^8 \text{TWI}_n \right) \quad (9)$$

This index differs from Index 4 because it does not remove the hypothesis of steady state.

The last index defined in this study is a second 'traditional topographic index' (TWI^{mf} , Index 6 in Table II), where the upslope contributing area (A_i^{mf}) was computed by using the dispersive multiple flow direction algorithm of Quinn *et al.* (1991):

$$\text{TWI}^{mf} = \log \left(\frac{A_i^{mf}/b_i}{\tan \beta_i} \right) \quad (10)$$

A_i^{mf} is computed by distributing the incoming upslope flow to every adjacent downslope cell on a slope-weighted basis. This method has been shown to be able to improve the computation of drainage areas and the description of flow paths over morphologically divergent terrains (e.g. Freeman, 1991; Quinn *et al.*, 1991) where hydrodynamic dispersion is generally highly relevant.

In the following sections, Index 1 (TWI) and Index 5 (TWI^{mf}) are termed 'traditional nondispersive topographic index TWI' (because it was computed by using Orlandini's path-based single flow routing method) and 'traditional dispersive topographic index TWI^{mf} ' (because it was computed by using Quinn's dispersive multiple flow routing method), respectively.

Performance criteria

The goal of our theoretical analysis was to assess the ability of the six wetness indices to reproduce water table

fluctuation (i.e. dynamics of water storage deficit) and subsurface flow paths derived from the physically based BEq model. Specifically, we tested the ability of each index to generate a clear contrast between wetter and drier zones. We used a spatially uniform representation of rainfall, hydraulic conductivity and soil porosity to run the BEq model to obtain predictions only affected by topography. The results are an emerging property of the model simulation and can be consistently compared with the spatial distribution of the terrain-based wetness indices defined in Table II.

Two approaches were used to compare wetness patterns derived from the BEq model with those derived from our terrain-based wetness indices. For the first approach (approach 1), reclassified binary maps with specific threshold values were used to differentiate between wetter and drier zones. For the second approach (approach 2), continuous data of terrain indices and water table levels (i.e. deficit of storage, according to TOPMODEL) derived by the BEq model were used. By using two different approaches, we were able to verify that our results were not dependent on the particular method used to classify the patterns of storage (binary versus continuous data). Six statistical measures were used to identify the level of similarity between wetness indices and simulated patterns of wetness/dryness: five similarity coefficients were used to assess the level of similarity in approach 1, whereas Spearman's rank correlation coefficient (Spearman, 1904) was used to assess the level of map similarity in approach 2.

To reclassify the original maps into binary (wetter/drier) maps, we rearranged the spatial distribution of values above or below a given threshold value by coding each value as an indicator function $I(z_i; z_k)$:

$$\begin{aligned} I(z_i; z_k) &= 1 \text{ if } z_i \geq z_k \\ I(z_i; z_k) &= 0 \text{ if } z_i < z_k \end{aligned} \quad (11)$$

where z_i is the value of wetness index or water table level in point i , and z_k is the threshold value that separates the drier areas from the wetter ones.

A second indicator datum $I(z_i; z_k)$ (such that $I(z_i; z_k) = 0$ if $z_i \geq z_k$ and $I(z_i; z_k) = 1$ if $z_i < z_k$) was also defined to guarantee the following condition:

$$\sum_N I(z_i; z_k) + \underline{I}(z_i; z_k) = N \quad (12)$$

where N is the total number of cells in the raster map. We used the 75th percentiles of the individual empirical cumulative distribution functions (ECDFs) to define the threshold value z_k and to separate the wetter areas from the drier ones. For comparison, we also used the 25th percentiles as indicator threshold z_k to assess the ability of the different terrain indices to include topographic divergent areas among the wetter zones.

The similarity coefficients used to assess the level of similarity of the binary maps (approach 1) are summarised in Table III (the case of the traditional topographic index

TWI is there reported). The overall probability of random agreement, RA, which appears in Cohen's kappa coefficient (C_k) is given by

$$\text{RA} = \frac{\sum_{i=1}^N I(\text{TWI}_i; \text{TWI}_{75\text{th}}) \times \sum_{i=1}^N I(\psi_i; \psi_{75\text{th}})}{N \times N} + \frac{\sum_{i=1}^N I(\text{TWI}_i; \text{TWI}_{75\text{th}}) \times \sum_{i=1}^N I(\psi_i; \psi_{75\text{th}})}{N \times N} \quad (13)$$

These five coefficients have been used in several similar studies (e.g. Rodhe and Seibert, 1999; Güntner *et al.*, 2004; Grabs *et al.*, 2009). λ and ν represent, respectively, the proportion of false-negative cases (i.e. the rate of occurrence to predict a 'drier' area when the BEq results in being a 'wetter' area) and false-positive cases (i.e. the rate of occurrence to predict a 'wetter' area when the BEq results in being a 'drier' area). The simple-matching (SM) coefficient specifies the percentage of catchment points where both the topographic index and the BEq-derived water-table depth (or storage deficit) predict values larger than their respective threshold values z_k . SC is a measure of direct spatial coincidence, and C_k (Cohen, 1960) is a coefficient able to take into account the agreement occurring by chance.

A modified version of the Hoshen–Kopelman algorithm (Hoshen *et al.*, 1997) was used to compute the number of 'wetter clusters' (i.e. spatial aggregates of value above the threshold z_k that separates the drier areas from the wetter ones) in the binary maps of the different terrain indices. We also determined the size of the 'wetter clusters' and their cumulative distribution function (ECDF_{size}). This was performed to assess the capacity of the different terrain indices (i) to separate wetter areas from surrounding drier areas and (ii) to reproduce the size of the isolated wetter clusters provided by the BEq model. The rationale behind this is that a high number of isolated clusters indicates limited ability of the wetness index to clearly separate the wetter areas from the drier areas.

RESULTS

The role of the diffusive term

The BEq model simulated the water-table depth (i.e. the water storage deficit) at each point in the Salei basin during the investigated rainfall events. We only present results of a 16-h-long, 4-mm h⁻¹ intense rainfall event because the qualitative results were the same for the other simulated rainfalls (a 16-h-long, 2-mm h⁻¹ intense rainfall and an 8-h-long, 6-mm h⁻¹ intense rainfall).

Figure 4 plots the drainage directions from the BEq-derived water-table surface ($\rightarrow(z_b + \psi)$) against the direction of the terrain gradient (or local slope) $\rightarrow(z_b)$. The four graphs refer to the 1st (top-left), 6th (top-right), 11th (bottom-left) and 16th hour (bottom-right) from the onset of rainfall. In Figure 4, the direction of $\rightarrow(z_b + \psi)$ was derived by using Orlandini's single flow path algorithm. The sizes of the circles indicate the percentage of catchment points characterised by a given pair of water table (in abscissa) and topographic drainage (in ordinate) directions. The red diagonal contains the percentage of catchment points where $\rightarrow(z_b + \psi)$ and $\rightarrow(z_b)$ present the same direction, whereas circles outside this diagonal represent the percentage of points where there is no coincidence.

The four graphs show that the direction of $\rightarrow(z_b + \psi)$ equals the direction of $\rightarrow(z_b)$ (i.e. that $\rightarrow(\psi) = 0$) in only 16% of the catchment-points, and that in many cases, the BEq-derived flow direction did not follow the topographic paths. In fact, although the topographic surface tended to establish three main drainage directions (northeast direction, southwest direction and southeast direction in 91.7% of cases), the direction of the subsurface flow (from the BEq model) resulted in a more complex variability across the watershed. The BEq-derived flow paths also exhibited a temporal variability induced by dynamic soil–water potential effects not captured by the static topography. Given that the flow directions are time variable, then the local values of storage deficit are also time variable.

Table III. An overview of the applied similarity coefficients (approach 1) and their theoretical range

Similarity coefficient	Formulation	Range
λ	$\frac{\sum_{i=1}^N I(\text{TWI}_i; \text{TWI}_{75\text{th}}) \cdot I(\psi_i; \psi_{75\text{th}})}{\sum_{i=1}^N I(\text{TWI}_i; \text{TWI}_{75\text{th}}) \times I(\psi_i; \psi_{75\text{th}}) + \sum_{i=1}^N I(\text{TWI}_i; \text{TWI}_{75\text{th}}) \times I(\psi_i; \psi_{75\text{th}})}$	[0,1]
μ	$\frac{\sum_{i=1}^N I(\text{TWI}_i; \text{TWI}_{75\text{th}}) \times I(\psi_i; \psi_{75\text{th}})}{\sum_{i=1}^N I(\text{TWI}_i; \text{TWI}_{75\text{th}}) \times I(\psi_i; \psi_{75\text{th}}) + \sum_{i=1}^N I(\text{TWI}_i; \text{TWI}_{75\text{th}}) \times I(\psi_i; \psi_{75\text{th}})}$	[0,1]
SM	$\frac{\sum_{i=1}^N I(\text{TWI}_i; \text{TWI}_{75\text{th}}) \cdot I(\psi_i; \psi_{75\text{th}}) + \sum_{i=1}^N I(\text{TWI}_i; \text{TWI}_{75\text{th}}) \cdot I(\psi_i; \psi_{75\text{th}})}{N}$	[0,1]
SC	$\frac{\sum_{i=1}^N I(\text{TWI}_i; \text{TWI}_{75\text{th}}) \times I(\psi_i; \psi_{75\text{th}})}{\sum_{i=1}^N I(\psi_i; \psi_{75\text{th}})}$	[0,1]
C_k	$\frac{\text{SM} - \text{RA}}{1 - \text{RA}}$	$[-\infty, 1]$

The case of the traditional dispersive TWI index is reported here.

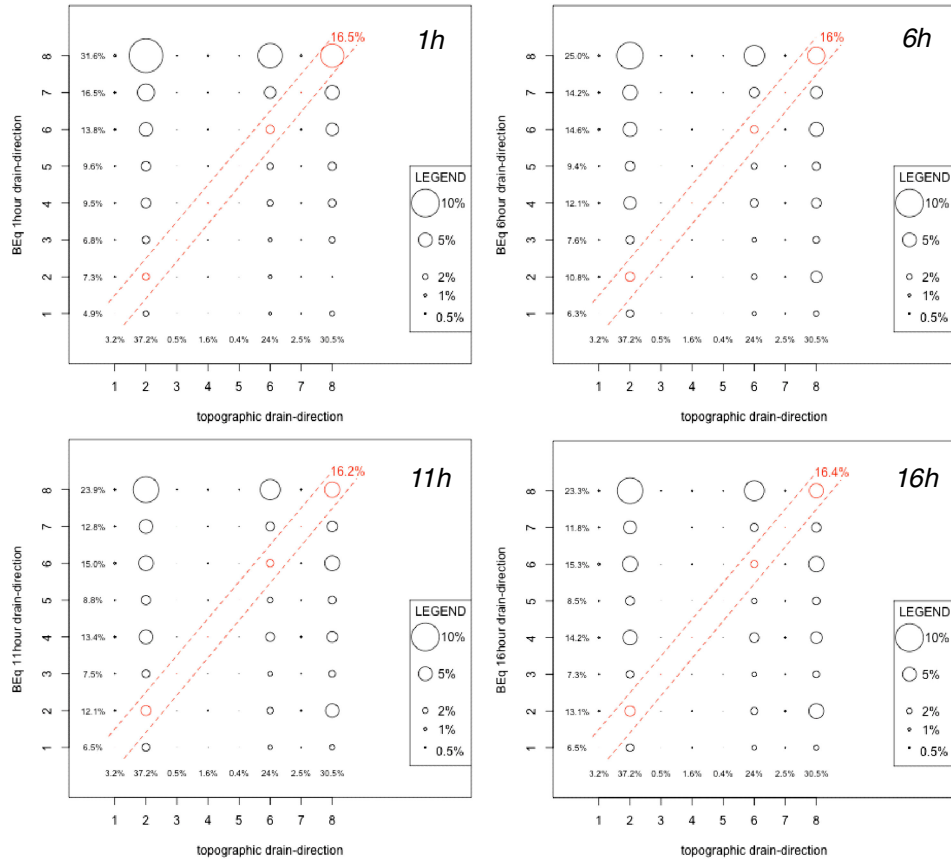


Figure 4. The direction of BEq-derived water table gradient $\rightarrow(z_b + \psi)$ against the direction of the topographic surface gradient $\rightarrow(z_b)$. Directions are coded with numbers ranging from 1 (east direction) to 8 (southeast direction), going counterclockwise. The percentages in the left and bottom inside margins of the plots represent the percentage of points characterised by a given value of water table drainage direction and topographic surface drainage direction, respectively

Figure 5 shows this effect of diffusive processes for a transect approximately perpendicular to the general direction of the topographic hollows (that can be considered representative of each other transect having the same direction). Along the transect, the surface topography and the BEq-derived water table surface were generally not parallel, particularly where the downslope topography induced backwater effects. A wedge of saturation developed near the topographic hollows and moved upslope from the foot of the slopes (points 1 and 2 noted on the transect of Figure 5b), inducing larger storage

in zones close to the hollows. Low saturation deficits were also present at some locations far from the hollows (e.g. at point 3), where downslope topographic reliefs limit the release of water from areas located upslope.

The performance of the terrain indices

Binary maps analysis (approach 1). Indicator map derivation showed that the smoothed dynamic topographic index TWI_d^* was able to reproduce the dynamics of storage (or water table depth) generated by the BEq model better than the other wetness indices listed in Table II. The visual

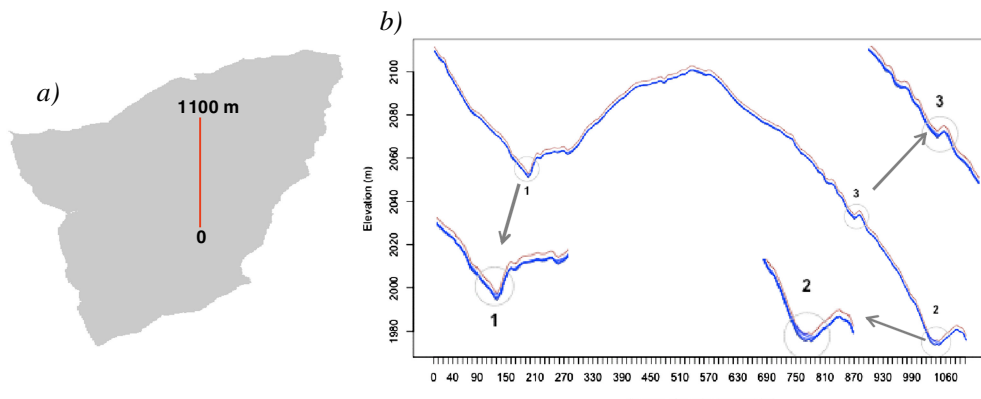


Figure 5. Two-dimensional transect of Salei catchment and simulated water-table level by BEq model. The red line in panel a shows the position of the transect reported in panel b. Low water storage deficit is observed near topographic hollows at the foot slope and where the irregular downslope topography prevents the free water drainage

comparison among the five maps in Figure 8 allows a preliminary qualitative assessment of pattern similarity. This comparison indicates that TWI_d^* (Figure 6d) is the most convincing index in describing similarity with the BEq-derived water storage patterns (Figure 6e).

The temporal evolution of the similarity coefficients λ , v , SM, SC and C_k between binary-coded terrain indices and simulated water table level are summarised in Tables IV and V. Table IV refers to $z_k = 75$ th percentile (i.e. the 75th percentile of the individual cumulative distribution functions was used as a threshold to separate wetter and drier areas), whereas Table V refers to $z_k = 25$ th percentile of the ECDFs. TWI_d approximated the BEq-derived storage deficit (or water table depth) most accurately during the first and second rainfall hours (values in bold face), whereas TWI_d^* performed better in subsequent hours if wetter and drier areas were separated by using $z_k = 75$ th percentile. TWI^{mf} was better able to approximate the BEq-derived wetter areas during the first five rainfall hours with $z_k = 25$ th percentile of the individual ECDFs, whereas TWI_d^* outperformed the other indices in the subsequent hours.

The traditional dispersive topographic index TWI consistently performed worse than the other indices in both cases ($z_k = 25$ th percentile and $z_k = 75$ th percentile of ECDFs), confirming the need to relax the steady-state assumption and to consider nonlocal factors (e.g. nonlocal topography) in describing the local drainage and storage dynamics. Tables IV and V also show that the similarity between TWI-BEq and TWI_d -BEq slightly decreases after the eighth rainfall hour, whereas the similarity between TWI^{mf} -BEq and TWI_d^* -BEq continued to increase until the last simulated hour when the diffusive processes are expected to become more relevant and the patterns of soil–water are highly connected and organised.

Spearman rank analysis (approach 2). In this second approach, Spearman's rank correlation coefficient ρ (Spearman, 1904) was used to assess the level of similarity

between terrain index and BEq-derived patterns of storage deficit (or water table depth).

Figure 7a shows the shift in performance of the dynamic TWI_d index and the smoothed dynamic TWI_d^* index (first 2 h versus the remaining), confirming the results obtained with approach 1 and $z_k = 75$ th percentile of the ECDFs (Table IV).

The dynamic topographic index defined by using the downslope index (DWI) and $d = 2$ m was the best index to approximate the BEq-derived patterns of storage deficit during the first three rainfall hours (Figure 7a). However, the use of downslope index, DWI, instead of local slope, $\tan\beta$, reduced the ability of the dynamic index to reproduce the simulated water-table levels (TWI_d^{DWI} less effective than TWI_d), especially when the higher values of d (5 and 10 m) were used to derive the DWI.

The traditional topographic index TWI was generally recognised as the least performing index, confirming what we found with approach 1. The performance of the terrain indices increased when the steady-state hypothesis was relaxed (TWI_d better than TWI, with an average increase of Spearman's coefficient equal to $\bar{\Delta}\rho = +9\%$) and when the low-pass filter was applied to the dynamic topographic indices TWI_d (TWI_d^* better than TWI_d with $\bar{\Delta}\rho = +17\%$).

Figure 7b shows that the ability of topographic indices to reproduce the patterns of soil–water storage deficit derived with the BEq model improved when the low-pass filter was used to smooth out local variations (TWI^* better than TWI, and TWI_d^* better than TWI_d). The traditional dispersive topographic index TWI^{mf} performed similarly to the smoothed traditional dispersive index TWI^* only from the 11th rainfall hour, when a considerable number of divergent areas also exhibited low saturation deficit. Figure 7b also shows that after the 8th rainfall hour Spearman's correlation coefficient ρ associated with TWI_d slightly decreases, whereas Spearman's correlation coefficient ρ associated with TWI_d^* increases to remain steady after the 13th hour. Besides, Spearman's correlation

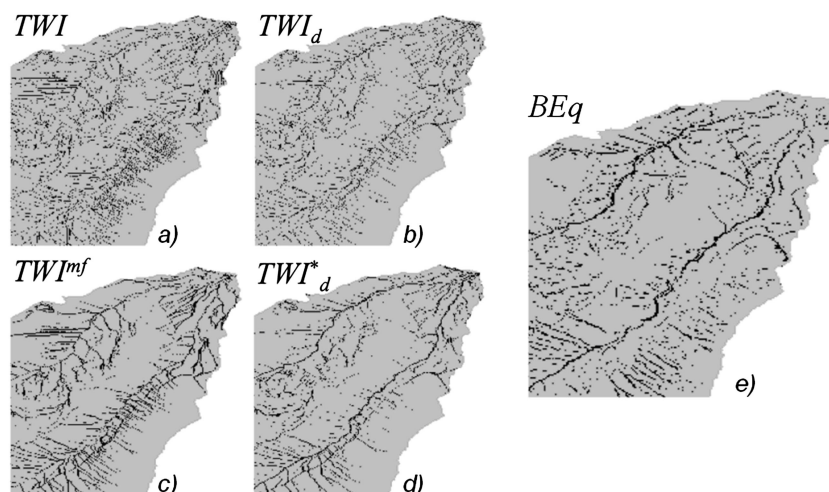


Figure 6. Spatial patterns of the (a) traditional 'nondispersive' topographic index TWI, (b) dynamic topographic index TWI_d , (c) traditional 'dispersive' topographic index TWI^{mf} , (d) smoothed dynamic topographic index TWI_d^* and (e) BEq-derived water table levels. The maps show in grey the points lower than the 75th percentile, and in black the points higher than the 75th percentile of the individual cumulative distribution functions

Table IV. Similarity coefficients between reclassified binary maps of wetness indices (TWI, TWI^{mf} , TWI_d and TWI_d^*) and simulated water table depth (or storage deficit) by BEq model with $z_k=75$ th percentile of the individual cumulative distribution functions

		Hour of imulation															
$z_k=75\%$	Label	1	2	3	4	5	6	7	8	9	10	11	12	13	14	15	16
λ	TWI	0.18	0.18	0.17	0.17	0.17	0.17	0.17	0.17	0.17	0.17	0.17	0.17	0.17	0.17	0.17	0.17
	TWI^{mf}	0.19	0.18	0.17	0.17	0.16	0.16	0.16	0.16	0.15	0.15	0.15	0.15	0.15	0.15	0.15	0.15
	TWI_d	0.16	0.15	0.15	0.14	0.14	0.14	0.14	0.14	0.14	0.14	0.14	0.14	0.14	0.14	0.15	0.15
	TWI_d	0.16	0.15	0.14	0.14	0.13	0.13	0.12	0.11	0.11							
v	TWI	0.55	0.53	0.52	0.51	0.50	0.50	0.51	0.51	0.51	0.51	0.51	0.51	0.51	0.51	0.51	0.51
	TWI^{mf}	0.57	0.54	0.52	0.50	0.49	0.48	0.48	0.47	0.47	0.46	0.46	0.46	0.46	0.46	0.46	0.45
	TWI_d	0.48	0.46	0.44	0.43	0.42	0.42	0.42	0.42	0.42	0.43	0.43	0.43	0.44	0.44	0.44	0.44
	TWI_d^*	0.49	0.46	0.43	0.41	0.39	0.38	0.37	0.37	0.36	0.36	0.36	0.36	0.36	0.35	0.35	
SC	TWI	0.45	0.47	0.48	0.49	0.49	0.49	0.49	0.49	0.49	0.49	0.49	0.49	0.49	0.49	0.48	0.48
	TWI^{mf}	0.43	0.46	0.48	0.49	0.51	0.52	0.52	0.53	0.53	0.54	0.54	0.54	0.54	0.54	0.54	0.54
	TWI_d	0.52	0.54	0.56	0.57	0.58	0.58	0.58	0.58	0.58	0.57	0.57	0.57	0.56	0.56	0.55	
	TWI_d	0.51	0.54	0.57	0.59	0.60	0.62	0.63	0.64								
SM	TWI	0.72	0.73	0.74	0.74	0.75	0.75	0.75	0.75	0.75	0.75	0.74	0.74	0.74	0.74	0.74	
	TWI^{mf}	0.71	0.73	0.74	0.75	0.76	0.76	0.76	0.77	0.77	0.77	0.77	0.77	0.77	0.77	0.77	
	TWI_d	0.76	0.77	0.78	0.79	0.79	0.79	0.79	0.79	0.79	0.79	0.79	0.78	0.78	0.78	0.78	
	TWI_d^*	0.75	0.77	0.78	0.79	0.8	0.81	0.81	0.82								
C_k	TWI	0.27	0.29	0.31	0.32	0.33	0.33	0.33	0.33	0.33	0.32	0.32	0.32	0.32	0.31	0.31	0.31
	TWI^{mf}	0.24	0.28	0.31	0.33	0.35	0.36	0.37	0.37	0.38	0.38	0.39	0.39	0.39	0.39	0.39	0.40
	TWI_d	0.36	0.39	0.42	0.43	0.44	0.45	0.45	0.44	0.44	0.43	0.43	0.42	0.42	0.41	0.41	
	TWI_d^*	0.34	0.38	0.42	0.45	0.48	0.49	0.50	0.51	0.52	0.52	0.53	0.53	0.53	0.53	0.53	

Values in bold represent the best index at a given rainfall hour.

coefficient ρ associated with TWI_d^* exceeded 0.7 after the 8th rainfall hour (approximately), indicating that the agreement between the index pattern and the simulated water table (or water storage deficit) pattern was good.

Connectivity analysis. The smoothed wetness index TWI_d^* and the traditional dispersive topographic index TWI^{mf}

showed better ability to generate a clear contrast between wetter and drier areas than the dynamic TWI_d index and the traditional nondispersive topographic TWI index (Figure 6). The analysis of the wetness patterns predicted by each of the wetness indices and the BEq model revealed that the number of wetter clusters (i.e. spatial aggregates of values larger than the threshold value z_k) generated by TWI_d^* and

Table V. Similarity coefficients between reclassified binary maps of wetness indices (TWI, TWI^{mf} , TWI_d and TWI_d^*) and simulated water table depth (or storage deficit) by BEq model with $z_k=25$ th percentile of the individual cumulative distribution functions

		Hour of simulation															
$z_k=25\%$	Label	1	2	3	4	5	6	7	8	9	10	11	12	13	14	15	16
λ	TWI	/	0.58	0.56	0.53	0.49	0.48	0.48	0.48	0.48	0.48	0.48	0.48	0.48	0.48	0.48	0.48
	TWI^{mf}	/	0.56	0.53	0.48	0.43	0.41	0.40	0.39	0.39	0.38	0.38	0.37	0.36	0.36	0.36	0.36
	TWI_d	/	0.58	0.54	0.50	0.47	0.45	0.44	0.44	0.44	0.45	0.45	0.46	0.46	0.47	0.47	0.48
	TWI_d^*	/	0.60	0.56	0.50	0.44	0.41	0.39	0.38	0.37	0.36	0.35	0.35	0.35	0.35	0.35	
v	TWI	0.25	0.19	0.19	0.18	0.17	0.16	0.16	0.16	0.16	0.16	0.16	0.16	0.16	0.16	0.16	0.16
	TWI^{mf}	0.25	0.19	0.18	0.16	0.14	0.14	0.13	0.13	0.13	0.13	0.12	0.12	0.12	0.12	0.12	0.12
	TWI_d	0.25	0.19	0.18	0.17	0.16	0.15	0.15	0.15	0.15	0.15	0.15	0.15	0.15	0.16	0.16	0.16
	TWI_d^*	0.25	0.20	0.19	0.17	0.15	0.14	0.13	0.13	0.12							
SC	TWI	0.75	0.80	0.81	0.82	0.83	0.84	0.84	0.84	0.84	0.84	0.84	0.84	0.84	0.84	0.84	0.84
	TWI^{mf}	0.75	0.81	0.82	0.84	0.85	0.86	0.87	0.87	0.87	0.87	0.88	0.88	0.88	0.88	0.88	0.88
	TWI_d	0.75	0.80	0.81	0.83	0.84	0.85	0.85	0.85	0.85	0.85	0.85	0.85	0.85	0.84	0.84	0.84
	TWI_d^*	0.75	0.80	0.81	0.83	0.85	0.86	0.87	0.87	0.88							
SM	TWI	0.75	0.70	0.72	0.74	0.75	0.76	0.76	0.76	0.76	0.76	0.76	0.76	0.76	0.76	0.76	0.76
	TWI^{mf}	0.75	0.72	0.73	0.76	0.78	0.79	0.80	0.80	0.81	0.81	0.82	0.82	0.82	0.82	0.82	0.82
	TWI_d	0.75	0.71	0.73	0.75	0.77	0.77	0.78	0.78	0.78	0.78	0.77	0.77	0.77	0.77	0.76	0.76
	TWI_d^*	0.75	0.70	0.72	0.75	0.79	0.80	0.81	0.82	0.82	0.82	0.82	0.82	0.82	0.83	0.83	
C_k	TWI	0	0.22	0.26	0.30	0.34	0.35	0.36	0.36	0.36	0.36	0.36	0.36	0.36	0.36	0.36	0.35
	TWI^{mf}	0	0.25	0.29	0.36	0.42	0.45	0.46	0.47	0.48	0.49	0.5	0.51	0.51	0.52	0.52	0.52
	TWI_d	0	0.22	0.27	0.33	0.37	0.40	0.41	0.41	0.41	0.40	0.39	0.38	0.38	0.37	0.36	
	TWI_d^*	0	0.20	0.25	0.34	0.41	0.45	0.48	0.49	0.51	0.52	0.53	0.53	0.53	0.53	0.53	

Values in bold represent the best index at a given rainfall hour.

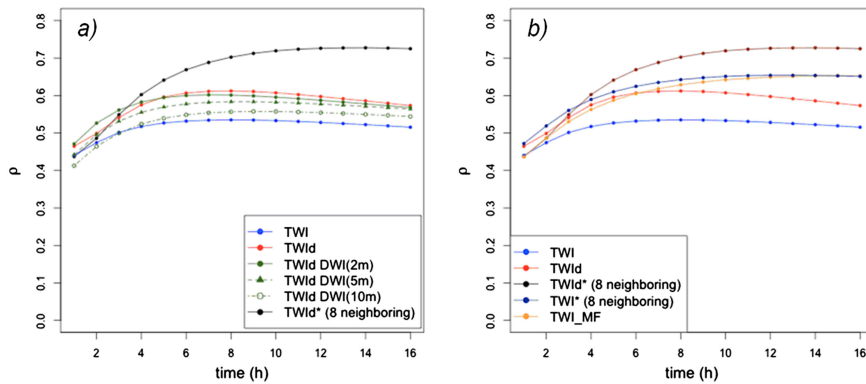


Figure 7. On the left, temporal evolution of Spearman's rank correlation coefficient ρ between simulated water table level and traditional non-dispersive topographic index, TWI (blue), dynamic topographic index, $TWId$ (red), smoothed dynamic topographic index, $TWId^*$ (black), and dynamic index where the DWI is used to describe the local drainage, $TWId^{DWI}$ (green). On the right, the role played by the low-pass filter on the terrain indices performance

TWI^{mf} was very close to the number of BEq-derived wetter clusters (Figure 8, rightmost bars-block). However, although the TWI^{mf} index generated connected patterns of wetter clusters too large, the $TWId^*$ index proved able to reproduce both the number of wetter clusters and the spatial aggregation of water storage patterns. In fact, the wetter clusters distribution from $TWId^*$ showed statistical properties (mean and quantiles values) that were in good agreement with the statistical properties of the BEq-derived wetter clusters distribution (Figure 8, first to fourth bars-blocks versus dashed lines).

TWI and TWI^* overestimated the fragmentation of the wetness areas, whereas the DWI-derived dynamic wetness index, $TWId^{DWI}$ (not reported in Figure 8), overestimated the clusters spatial extension and underestimated the number of clusters for high values of 'loss of elevation' d (5 and 10 m) and, *vice versa*, underestimated the clusters spatial extension and overestimated the number of clusters for $d=2$ m.

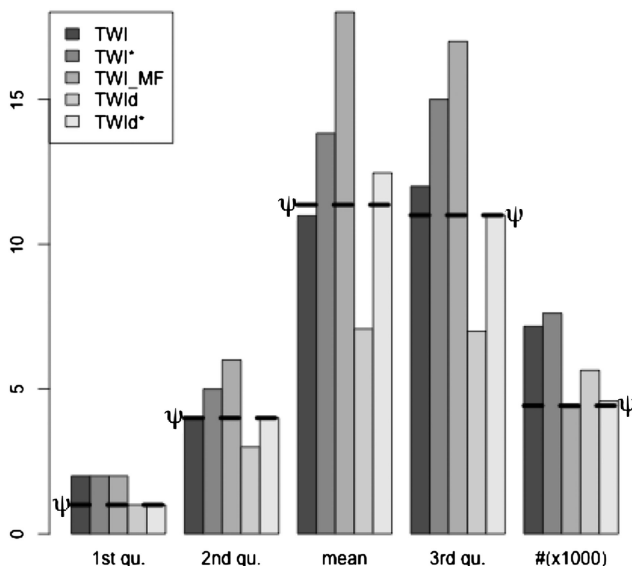


Figure 8. Bar plots showing the ability of the different terrain indices to reproduce connected 'wetter' areas. The rightmost bars-block represent the number of isolated 'wetter' clusters provided by the five (TWI, TWI^* , TWI^{mf} , $TWId$ and $TWId^*$) terrain indices (bars) and the BEq model (dashed line). The first, second, third and fourth bars-blocks represent the 1st quantile, 2nd quantile, mean and 3rd quantile values of the individual cumulative distribution functions of the 'wetter' cluster sizes

DISCUSSION

On the relative role of upslope and downslope topography for describing water flow path, connectivity and storage dynamics

The use of a TWI for distributing soil–water storage imposes an inherent assumption about the controlling processes on subsurface flow dynamics, namely, that subsurface lateral flow dominates (e.g. Grayson *et al.*, 1997). The results of our theoretical analysis have shown that diffusive, pressure related, processes can significantly affect the subsurface lateral flow dynamics (Figures 4 and 5) and that the traditional topographic index alone is a poor proxy for describing subsurface flow paths and storage dynamics over complex topography. The steady-state assumption, which implies that the storage deficit at any point in a catchment is influenced by the total upslope contributing area, and the kinematic-wave theory, whereby the effects of disturbance can only propagate in a downslope direction, limit the ability of the traditional TWI index to describe storage dynamics in topographically complex, lateral flow-dominated mountain catchments.

Water storage deficit at a given location may in fact be strongly controlled by the downslope topography. Very steep and planar downslope topography enhances the local drainage, independently of the local value of the ratio between upslope contributing area and local slope. On the other hand, an abrupt decrease in slope angle or the presence of micro-topographic reliefs may prevent the free water drainage, inducing backwater effects. A saturation wedge may also develop at the foot of the hillslope and affect the upslope storage dynamics for a length depending upon the incoming flux from upslope (Hewlett and Hibbert, 1963; Weyman, 1973, 1974). This mechanism can be intimately related to the hydrological connectivity between the topographic channel and the surrounding hillslopes, and it is not considered at all in the TWI index where downslope controls on local drainage are neglected. Therefore, rainfall-runoff models on the basis of the traditional topographic index to describe the lateral subsurface flow component (i.e. the balance between the incoming upslope flow and the outgoing downslope flow) are not able to fully represent storage dynamics, at least for the right reasons, where

downslope topography and soil water potential effects play an important role in controlling the local drainage.

On the need for hydrological smearing

None of the six terrain indices tested in this study were able to perfectly reproduce the dynamics of storage derived from the Boussinesq model. This is because none of them perfectly captures the hydrodynamic processes induced by the irregular and complex topography. The downslope index DWI attempts to include elements of the downslope topography to describe the local drainage propensity. However, our results have shown that the DWI is difficult to apply in practice. The effective value of d (loss of elevation), a crucial element of the DWI method, must be chosen by trial and error—as a single value for the entire watershed—based on what local micro-topographic features (i.e. local irregularities) must be filtered out. Therefore, the value of d changes as a function of local morphology and is not a topological property of a basin.

The traditional dispersive topographic index TWI^{mf} attempts to include the hydrodynamic processes by distributing the incoming flow (i.e. the routed upslope contributing area) to a point among the neighbouring cells at a lower elevation. This enabled it to better estimate water storage in divergent areas (Table V), but at the same time, TWI^{mf} showed poor performance with respect to the other tested quality measures (and specifically Spearman's correlation coefficient analysis and connectivity analysis). Orlandini and Moretti (2009) showed that multiple flow direction algorithms are not able to delineate the morphological drainage system because physical dispersion inherent in transport processes across the topographic surface may not obey the same laws as artificial dispersion. Our results support their findings by showing that a 3×3 low-pass filter applied on the traditional nondispersive TWI index was sufficient to outperform the dispersive TWI^{mf} index in approximating the BEq-derived water storage dynamics. In particular, TWI^{mf} showed small differences between convergent and divergent areas in the first rainfall hours when 'wetter' cells were primarily areas of flow convergence (Figure 6, Table IV). This confirmed that multiple flow direction algorithms suffer from too high flow dispersion (Seibert and McGlynn, 2007), making it unable to reproduce subsurface flow paths in convergent areas.

Fine DEM grids create challenges for the TWI. Small-scale topographic 'noise' generates high spatial variability in the ratio between upslope contributing area and local slope, reducing the ability of topographic index-based rainfall-runoff models to predict spatial patterns and dynamics of water storage. The problem has been noted by other researchers. For instance, Sørensen and Seibert (2007) argued that the water table shape may be smoother than the land surface topography and may be related more accurately to a coarse resolution DEM than to a finer resolution DEM. Wolock and Price (1994) concluded that coarse resolution DEMs were preferable to run the topographic index-based TOPMODEL as the predicted water-table shape may be better represented by a coarser

resolution DEM. Lane *et al.* (2004) showed results that could be considered similar to ours. They argued that when fine-resolution DEMs are used to run TOPMODEL, a large number of unconnected saturated areas are produced. This is similar to our findings of high disaggregation of points observed in the traditional nondispersive topographic index TWI and the dynamic index TWI_d (Figures 6a and 6b).

The values of upslope contributing areas for the Salei basin were greatly affected by the DEM resolution (confirming results by Sørensen and Seibert, 2007). For example, the percentage of basin points having an upslope contributing area larger than 160 m^2 increased from 18% at 2-m resolution to 70% at 10-m resolution DEM. Therefore, the coarse 10-m scale remains inappropriate to delineate water flow paths. In fact, our smoothed dynamic index TWI_d^* was poorly correlated with the BEq-derived storage deficit patterns when applied to this 10-m resolution DEM, indicating that a fine-resolution DEM is a necessary element to compute our TWI_d^* and appropriate times of concentration τ_c . The 3×3 low-pass filter subsequently applied to the dynamic topographic index maps mitigated the effects of local irregularities in topography and allowed us to include nonlocal topographic effects in the terrain index computation. This resulted in less fragmented and more robust patterns of wetness (Figure 6).

We found that the smearing process also allowed the reduction of the differences in the upslope contributing area between points near and points inside topographic hollows (spatial-threshold effect). Figure 9 provides a schematic representation of this spatial-threshold effect at the hillslope/channel transition. On 'digital terrain', points inside topographic hollows show values of upslope contributing area that are much higher than points immediately upslope. This effect is in contrast with the results of the BEq model (Figure 5), which showed a similar water-storage propensity for topographic positions close to and inside the topographic hollows. In fact, as discussed earlier, in points close to the hollows, local water storage is strongly controlled by the development of a saturated wedge that progressively expands in the upslope direction. As a result, locations near topographic hollows may receive drainage not only from areas that are directly upslope from them but downslope from them too.

Our smoothed dynamic index TWI_d^* has proven more capable to include these phenomena than existing topographic indices. However, it remains a terrain-derived index and as such can be used to describe the dynamics of storage only when topography (i.e. lateral subsurface flow) is recognised as the predominant control on subsurface flow mechanisms. Under different landscape contexts from those analysed in this article, storage dynamics and soil-moisture patterns can be dominated by other factors, such as soil drainability (Tetzlaff *et al.*, 2009a), vegetation and microclimate (Western *et al.*, 2004) and bedrock geology, where a realistic representation of storage patterns and storage dynamics cannot be achieved by using a solely terrain-based wetness index. In these cases, appropriate procedures should be used to select the requisite level of hydrological model complexity able to represent the

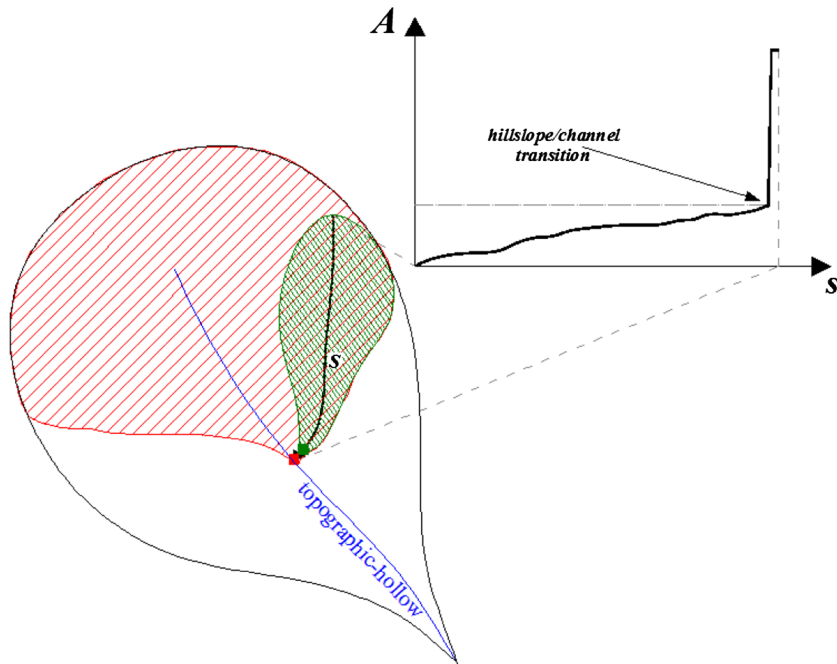


Figure 9. Conceptual representation of the threshold effect on the value of upslope contributing area at the hillslope/channel transition of digitised watersheds. The point inside the topographic hollow shows a value of upslope contributing area A much higher than a points located one pixel upslope

dominant processes (Fenicia *et al.*, 2008), consistent with empirical observations (Birkel *et al.*, 2010, and 2011).

CONCLUDING REMARKS

The position of the water table and the storage deficit below saturation at a given point in a watershed is the result of a balance between upslope accumulation of water, downslope drainage efficiency and vertical recharge from the unsaturated zone—all interplaying with the complexities of bedrock surface and permeability below. In a context where lateral flow in the soil layer dominates, we showed that downslope topography significantly affects the propensity of a point to retain or release water and therefore alters the flow and storage dynamics of upslope points. Our analysis allowed us (i) to examine the relative effects of advective (i.e. topographic) and diffusive (pressure dependent) flow processes by using a physically based BEq solver and (ii) to test the ability of several terrain-based wetness indices to approximate the BEq-derived water storage dynamics.

We showed that locally computed topographic wetness indices were not able to account for the role that complex topography plays on storage dynamics. Specifically, they were not able to represent the effect of downslope topography on upslope water flow. Results also highlighted the need to relax the steady-state assumption on which traditional topographic indices are based. Our new terrain index (TWI_d) applies a 3×3 low-pass filter to the dynamic index of Barling *et al.* (1994) to smooth out the effects of local topography and grid influence on water flow paths (i.e. the artefacts on flow paths connected to the use of a regular grid) and, ultimately, to derive a smoothed dynamic terrain index (TWI_d^*). Our statistical comparison showed that TWI_d^* outperformed previous indices when working with high-resolution DEMs, resulting in a less

fragmented and disconnected water table configuration. This was achieved without losing the accuracy afforded by high-resolution DEMs to describe drainage paths and upslope accumulated area. Moreover, because the TWI_d^* uses the concept of time-variable upslope contributing area, it is not limited by a single value, monotonic function between groundwater storage and runoff production.

Because many rainfall-runoff models rely upon these indices to cope with the spatial distribution and the dynamics of soil–water storage in a catchment, our new TWI_d^* index may be a better alternative to the traditional topographic index in describing subsurface flow processes, at least where topography (i.e. lateral flow) is recognised as the predominant control for subsurface flow mechanisms.

ACKNOWLEDGEMENTS

The authors thank T. Garland and E. Cordano for their comments on an earlier draft. E. Farabegoli and A. Vigano are thanked for their field work and for providing useful information in the geological context. The authors also thank S. Orlandini, G. Moretti and M. Borga for helpful discussions. They are grateful to the three anonymous reviewers for comments that improved the quality of this manuscript. All the codes presented in the article were implemented in R and are freely available by contacting the first author (cristiano.lanni@gmail.com).

REFERENCES

- Barling RD, Moore ID, Grayson RB. 1994. A quasi-dynamic wetness index for characterizing the spatial distribution of zones of surface saturation and soil water content. *Water Resources Research* **30**(4): 1029–1044. DOI: 10.1029/93WR03346.

- Bear J. 1972. Dynamics of Fluids in Porous Materials. Elsevier: New York (reprinted by Dover Publications, 1988).
- Beven KJ, Kirkby MJ. 1979. A physically based variable contributing area model of basin hydrology. *Hydrology Science Bulletin* **24**(1): 43–69.
- Beven K, Freer J. 2001. A dynamic TOPMODEL. *Hydrological Processes* **15**: 1993–2011. DOI: 10.1002/hyp.252.
- Birkel C, Tetzlaff D, Dunn SM, Soulsby C. 2010. Towards simple dynamic process conceptualization in rainfall runoff models using multi-criteria calibration and tracers in temperate, upland catchments. *Hydrological Processes* **24**: 260–275.
- Birkel C, Tetzlaff D, Dunn SM, Soulsby C. 2011. Using time domain and geographic source tracers to conceptualise streamflow generation processes in lumped rainfall-runoff models. *Water Resources Research* **47**: W02515. DOI: 10.1029/2010WR009547.
- Borga M, Dalla Fontana G, Cazorzi F. 2002. Analysis of topographic and climatologic control on rainfall-triggered shallow landsliding using a quasi-dynamic wetness index. *Journal of Hydrology* **268**: 56–71.
- Borga M, Dalla Fontana G, Da Ros D, Marchi L. 1998. Shallow landslide hazard assessment using a physically based model and digital elevation data. *Environmental Geology* **35**(2): 81–88. DOI: 10.1007/s002540050295.
- Brugnano L, Casulli V. 2009. Iterative Solution of Piecewise Linear Systems and Applications to Flows in Porous Media. *SIAM Journal on Scientific Computing* **31**: 1858–1873.
- Burt TP, Butcher DP. 1986. Development of topographic indices for use in semi-distributed hillslope runoff models. *Zeitschrift für Geomorphologie* **58**: 1–19.
- Burt TP, Butcher DP. 1985. Topographic controls of soil moisture distributions. *Journal of Soil Science* **36**: 469–486.
- Carson MA, Kirkby MJ. 1972. Hillslope form and process. University Press: Cambridge, England; 475.
- Cohen J. 1960. A coefficient of agreement for nominal scales. *Educational and Psychological Measurement* **20**: 37–46.
- Cordano E, Rigon R. submitted. A mass-conservative method for the integration of the two-dimensional groundwater (Boussinesq) equation. *Water Resources Research*.
- Crave A, Gascuel-Odoux C. 1997. The influence of topography on time and space distribution of soil surface water content. *Hydrological Processes* **11**: 203–210.
- Fenicia F, McDonnell JJ, Savenije HHG. 2008. Learning from model improvement: On the contribution of complementary data to process understanding. *Water Resources Research* **44**: W06419. DOI: 10.1029/2007WR006386.
- Freeman TG. 1991. Calculating catchment area with divergent flow based on regular grid. *Computers and Geosciences* **17**: 413–422.
- Gallant JC, Hutchinson MF. 2011. A differential equation for specific catchment area. *Water Resources Research* **47**. DOI: 10.1029/2009WR008540.
- Grabs T, Seibert J, Bishop K, Laudon H. 2009. Modeling spatial patterns of saturated areas: A comparison of the topographic wetness index and a dynamic distributed model. *Journal of Hydrology* **373**(1–2): 15–23.
- Grayson RB, Western AW, Chiew FHS, Blöschl G. 1997. Preferred states in spatial soil moisture patterns: local and nonlocal controls. *Water Resources Research* **33**(12): 2897–2908. DOI: 10.1029/97WR02174.
- Güntner A, Seibert J, Uhlenbrook S. 2004. Modeling spatial patterns of saturated areas: An evaluation of different terrain indices. *Water Resources Research* **40**. DOI: 10.1029/2003WR002864.
- Haitjema HM, Mitchell-Bruker S. 2005. Are water tables a subdued replica of the topography? *Ground Water* **43**(6): 781–786.
- Hewlett JD, Hibbert AR. 1963. Moisture and energy conditions within a sloping soil mass during drainage. *Journal of Geophysical Research* **68**: 1081–1087.
- Hjerdt KN, McDonnell JJ, Seibert J, Rodhe A. 2004. A new topographic index to quantify downslope controls on local drainage. *Water Resources Research* **40**: W05602. DOI: 10.1029/2004WR003130.
- Hoshen J, Berry MW, Minser KS. 1997. Percolation and cluster structure parameters: The enhanced Hoshen-Kopelman algorithm. *Physical Review E* **56**(2): 1455–1460.
- Iorgulescu I, Jordan JP. 1994. Validation of TOPMODEL on a small Swiss catchment. *Journal of Hydrology* **159**(1–4): 255–273. DOI: 10.1016/0022-1694(94)90260-7.
- Jordan JP. 1994. Spatial and temporal variability of stormflow generation processes on a Swiss catchment. *Journal of Hydrology* **153**(1–4): 357–382. DOI: 10.1016/0022-1694(94)90199-6.
- Kirkby M. 1975. Hydrograph modelling strategies. In *Processes in Physical and Human Geography*, Peel R et al. (eds). Heinemann: London; 69–90.
- Lamb R, Beven KJ, Myrabo S. 1998. Use of spatially distributed water table observations to constrain uncertainty in a rainfall-runoff model. *Advances in Water Resources* **22**(4): 305–317.
- Lane SN, Brookes CJ, Kirkby MJ, Holden J. 2004. A network-index-based version of TOPMODEL for use with high-resolution digital topographic data. *Hydrological Processes* **18**: 191–201. DOI: 10.1002/hyp.5208.
- McGuire KJ, McDonnell JJ, Weiler M, Kendall C, McGlynn BL, Welker JM, Seibert J. 2005. The role of topography on catchment-scale water residence time. *Water Resources Research* **41**: W05002. DOI: 10.1029/2004WR003657.
- Montgomery DR, Dietrich WE. 1994. A physically based model for the topographic control on shallow landsliding. *Water Resources Research* **30**(4): 1153–1171. DOI: 10.1029/93WR02979.
- O'Callaghan JF, Mark DM. 1984. The extraction of drainage networks from digital elevation data. *Computer Vision, Graphics and Image Processing* **28**(3): 323–344. ISSN 0734-189X, DOI: 10.1016/S0734-189X(84)80011-0.
- Orlandini S, Moretti G. 2009. Determination of surface flow paths from gridded elevation data. *Water Resources Research* **45**: W03417. DOI: 10.1029/2008WR007099.
- Orlandini S, Moretti G, Franchini M, Aldighieri B, Testa B. 2003. Path-based methods for the determination of nondispersive drainage directions in grid-based digital elevation models. *Water Resources Research* **39**(6): 1144. DOI: 10.1029/2002WR001639.
- Pellenq J, Kalma J, Boulet G, Saulnier G-M, Wooldridge S, Kerr Y, Chehbouni A. 2003. A disaggregation scheme for soil moisture based on topography and soil depth. *Journal of Hydrology* **276**: 112–127.
- Quinn PF, Beven KJ, Chevallier P, Planchon O. 1991. The prediction of hillslope flowpaths for distributed modelling using digital terrain models. *Hydrological Processes* **5**: 59–80.
- Rigon R, Bertoldi G, Over TM. 2006. GEOTop: A distributed hydrological model with coupled water and energy budgets. *Journal of Hydro-meteorology* **7**(3): 371–388.
- Rodhe A, Seibert J. 1999. Wetland occurrence in relation to topography - a test of topographic indices as moisture indicators. *Agricultural and Forest Meteorology* **98–99**: 325–340.
- Seibert J, Bishop KH, Nyberg L. 1997. A test of TOPMODEL's ability to predict spatially distributed groundwater levels. *Hydrological Processes* **11**: 1131–1144.
- Seibert J, McGlynn BL. 2007. A new triangular multiple flow-direction algorithm for computing upslope areas from gridded digital elevation models. *Water Resources Research* **43**: W04501. DOI: 10.1029/2006WR005128.
- Sørensen R, Seibert J. 2007. Effects of DEM resolution on the calculation of topographical indices: TWI and its components. *Journal of Hydrology* **347**: 79–89.
- Spearman C. 1904. The proof and measurement of association between two things. *The American Journal of Psychology* **15**: 72–101.
- Stieglitz M, Shaman J, McNamara J, Engel V, Shanley J, Kling GW. 2003. An approach to understanding hydrologic connectivity on the hillslope and the implications for nutrient transport. *Global Biogeochemical Cycles* **17**(4): 1105. DOI: 10.1029/2003GB002041.
- Tarboton DG. 1997. A new method for the determination of flow directions and upslope areas in grid digital elevation models. *Water Resources Research* **33**(2): 309–319.
- Tarolli P, Borga M, Dalla Fontana G. 2008. Analysing the influence of upslope bedrock outcrops on shallow landsliding. *Geomorphology* **93**(3–4): 186–200.
- Tetzlaff D, Seibert J, McGuire KJ, Laudon H, Burns DA, Dunn SM, Soulsby C. 2009a. How does landscape structure influence catchment transit times across different geomorphic provinces? *Hydrological Processes* **23**: 945–953.
- Tetzlaff D, Seibert J, Soulsby C. 2009b. Inter-catchment comparison to assess the influence of topography and soils on catchment transit times in a geomorphic province: the Cairngorm mountains, Scotland. *Hydrological Processes* **23**: 1874–1886. DOI: 10.1002/hyp.7318.
- Western AW, Grayson RB, Blöschl G, Willgoose GR, McMahon TA. 1999. Observed spatial organization of soil moisture and its relation to terrain indices. *Water Resources Research* **35**(3): 797–810. DOI: 10.1029/1998WR900065.
- Western AW, Zhou SL, Grayson RB, McMahon TA, Blöschl G, Wilson DJ. 2004. Spatial correlation of soil moisture in small

- catchments and its relationship to dominant spatial hydrological processes. *Journal of Hydrology* **286**(1–4): 113–134. DOI: 10.1016/j.jhydrol.2003.09.014.
- Weyman DR. 1973. Measurements of the downslope flow of water in a soil. *Journal of Hydrology* **20**(3): 267–288. DOI: 10.1016/0022-1694(73)90065-6.
- Weyman DR. 1974. Runoff processes, contributing area and streamflow in a small upland catchment. In *Fluvial Processes in Instrumented Watersheds*, Gregory KJ, Walling DE (eds). Institute of British Geographers: London; 33–43.
- Wolock, DM, Price CV. 1994. Effects of digital elevation model map scale and data resolution on a topography-based watershed model. *Water Resources Research* **30**(11): 3041–3052. DOI: 10.1029/94WR01971.